

VORTEX/FLAME INTERACTIONS IN MICROGRAVITY PULSED JET DIFFUSION FLAMES

M. Y. Bahadori, Science and Technology Development Corporation; U. Hegde, National Center for Microgravity Research; and D. P. Stocker, NASA Glenn Research Center

INTRODUCTION

Significant differences have been observed between the structure of laminar, transitional, and turbulent flames under downward, upward, and microgravity conditions (Fig. 1). These include flame height, jet shear layer, flame instability, flicker, lift-off height, blow-off Reynolds number, and radiative properties [1-4]. The primary objective of this investigation is to identify the mechanisms involved in the generation and interaction of large-scale structures in microgravity flames. This involves a study of vortex/flame interactions in a space-flight experiment utilizing a controlled, well-defined set of disturbances imposed on a laminar diffusion flame. The results provide a better understanding of the naturally occurring structures that are an inherent part of microgravity turbulent flames. The paper presents the current progress in this program.

APPROACH

TGDF (Turbulent Gas Jet Diffusion Flames) is a self-contained, autonomous experiment which was flown in the cargo bay of the Space Shuttle *Columbia* during the STS-87 mission. Data on temperature field, radiative loss, and flame characteristics under pulsed conditions were obtained [5]. The imposed vortices were generated by periodically varying the open diameter of an iris located around the flame base. Figure 2 shows a comparison between smoke visualization of the vortex interacting with the flow field and the pulsed flame image in microgravity. A microgravity laminar propane diffusion flame burning in quiescent air was studied. The nozzle had an internal diameter of 1.65 mm, and the fuel was injected at $Re \cong 400$. The iris pulse frequency was in the 1-10 Hz range. Details of the experiment procedure are presented elsewhere [5]. A transient numerical model was developed to study the interaction of imposed vortices with the flame front. Figure 3 depicts the effects of disturbances on the temperature contour of the microgravity flame, and shows vortex-induced enhanced temperature zones. In addition, similar tests were conducted in normal gravity, and the effects of pressure were also studied.

RESULTS AND DISCUSSION

Analysis of the temperature-field oscillations provided insight into the vortex/flame interaction phenomenon. Figure 4 shows the normalized temperature oscillation for two locations inside the flame. It is seen that the phase difference is about 60° - 70° , i.e., oscillations are in-phase. In addition, it was found that for thermocouples located on both sides of the flame front, the flame movement causes the temperature oscillation to be almost 180° out of phase. As the flame gets closer to one thermocouple, its temperature rises, while the other thermocouple shows a drop in temperature. Therefore, oscillation phase-change occurs across the flame surface upon interaction of the vortex with the flame sheet. The axial variation of the temperature amplitude also shows some unique characteristics. Figure 5 compares the predicted and measured normalized centerline temperature for three axial locations. As the distance from the nozzle exit increases, the amplitude decreases. This is caused by oscillation decay and viscous dissipation. The observed phase lag for the locations along the centerline are related to the local convection velocity of the oscillations, and are shown to be in agreement with the computations[5]. As seen in Fig. 5, the predicted and measured centerline temperature oscillations, amplitude variation, and phase variation are in good agreement. Temporal variations of the velocity field have provided information on entrainment Figure 6 shows the

predicted instantaneous radial velocity field (i.e., $v = V + v'$) at three separate times during one cycle of the iris pulsing. In the lower part, near $x/d = 0$, the radial velocity is directed inward due to air entrainment, whereas in the upper part, the radial velocity is directed outward due to jet spreading. The dividing streamline, which represents the demarcation between these two regions, is also shown. In Fig. 6(b), the iris is moving inward towards its minimum open position, and the entrainment region becomes more dominant compared to that in Fig. 6(a) where the iris is near its maximum open position. The entrainment then reduces in the other part of the cycle, where the iris is moving outward in Fig. 6(c). The predicted field of the oscillatory component of radial velocity (i.e., v') is shown in Fig. 7. The iris is moving in from its maximum open position in Fig. 7(a), and the inward velocity is dominant near the flame base, whereas outward radial-velocity component is present further downstream. Once the iris approaches its minimum open position in Fig. 7(b), the amplitude of v' increases in the flame lower part. In Fig. 7(c), the iris is moving outward, and the flame base shows an outward direction of v' .

The effects of nonlinear interactions between the imposed pulsations and the flame flicker were also studied. The axial variation of the temperature autospectrum with and without pulsing in normal gravity is shown in Fig. 8. The autospectra depicted in Fig. 8(a) show that the flicker amplitude increases up to the location x_2 (which is near the normal-gravity flame tip), and then begins to decay at further downstream locations x_3 and x_4 . In the presence of pulsing, as seen in Fig. 8(b) for $f = 3$ Hz, while the flicker amplitude increases up to the flame tip and then begins to decrease, the amplitude peak is considerably broadened. This shows the presence of nonlinear interaction between the imposed pulsations and the flame flicker. The flicker frequency in normal gravity has approximately a square-root dependence on both pressure and gravitational level (e.g., [4]). Hence, it was of interest to analyze a normal-gravity flame under reduced-pressure condition. Figure 9 shows the variation of the centerline temperature amplitude at the pulse frequency of 1.5 Hz for the three cases of (a) Microgravity flame at 1 atm, (b) normal-gravity flame at 1 atm, and (c) normal-gravity flame at 0.5 atm. The axial decay behavior in the three cases is significantly different. The relative amplitude of the normal-gravity oscillation at 1 atm decays initially, but then grows in the downstream regions in contrast to the microgravity case at 1 atm and the normal-gravity case at 0.5 atm. This different behavior is caused by a number of factors such as buoyant acceleration, effects of flicker, and nonlinear interactions between buoyant instabilities and imposed oscillations.

ACKNOWLEDGMENTS

This work was supported by the NASA John H. Glenn Research Center under Contract NAS3-98031 (with STDC) and Cooperative Agreement NCC3-544 (with NCMR).

REFERENCES

- [1] Bahadori, M. Y., Stocker, D. P., Vaughan, D. F., Zhou, L., and Edelman, R. B., "Effects of Buoyancy on Laminar, Transitional, and Turbulent Gas Jet Diffusion Flames," Modern Developments in Energy, Combustion, and Spectroscopy, pp. 49-66, (F.A. Williams, A.K. Oppenheim, D.B. Olf, and M. Lapp, eds.), Pergamon Press, New York, 1993.
- [2] Hegde, U., Zhou, L., and Bahadori, M. Y., "The Transition to Turbulence of Microgravity Gas Jet Diffusion Flames," Combust. Sci. Tech., Vol. 102, pp. 95-113 (1994).
- [3] Bahadori, M. Y., Stocker, D. P., Zhou, L., and Hegde, U., "Radiative Loss from Non-Premixed Flames in Reduced-Gravity Environments," Combust. Sci. Tech., in press (2001).
- [4] Bahadori, M. Y., Zhou, L., Stocker, D. P., and Hegde, U., "Functional Dependence of Flame Flicker on Gravitational Level," AIAA Journal, in press (2001).
- [5] Hegde, U., Bahadori, M.Y., and Stocker, D.P., "Oscillatory Temperature Measurements in a Pulsed Microgravity Diffusion Flame," AIAA Journal, Vol. 38, pp. 1219-1229 (2000).

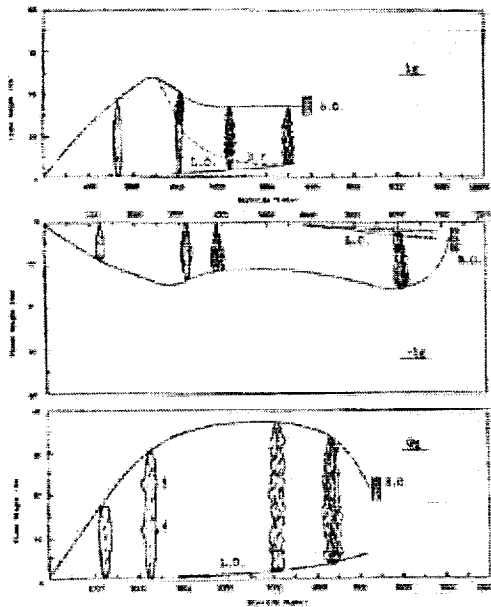


Fig. 1. Laminar, transitional, and turbulent propagating flame characteristics in normal gravity (1g), inverted gravity (-1g), and microgravity (0g) environments.

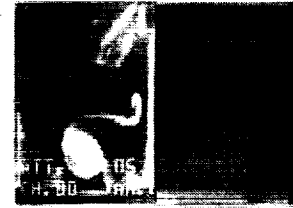


Fig. 2. Smoke visualization of the imposed vortex (left) and microgravity flame image (right).



Fig. 3. Predicted temperature contours (left) and flame surface (right). Note regions of vortex-induced enhanced temperature (in red) at the flame surface.

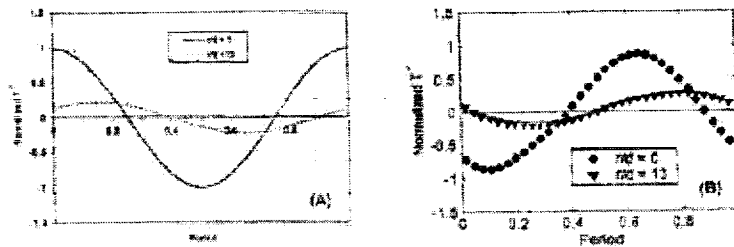


Fig. 4. Normalized temperature oscillations from (a) predictions, and (b) flight experiment, during one oscillation cycle at the same pulse frequency. The data and predictions are presented for the same axial location $x/d = 35$. Both thermocouples are on the same side of the flame sheet.

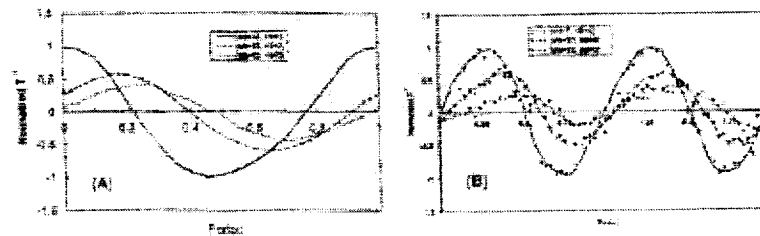


Fig. 5. Axial variation of the temperature amplitude along the flame centerline at the same oscillation frequency from (a) numerical model and (b) flight experiment. The normalized centerline temperatures are shown for three axial locations.

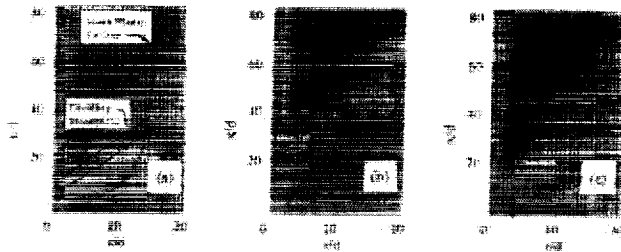


Fig. 6. Predicted instantaneous radial velocity distribution during one cycle of oscillation. Blue represents radially inward direction of velocity, and red represents radially outward direction. The mean flame surface location and the dividing streamline are noted in (a) the iris is moving in from its maximum open position in (a), is moving inward in (b), and is moving outward in (c).

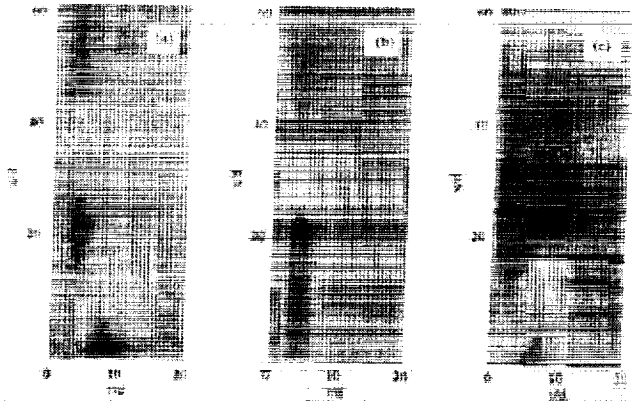


Fig. 7. Predicted flow structure during one cycle of pulsation obtained from the oscillatory component of the radial velocity. Blue indicates inward direction of radial velocity and red indicates outward direction. The iris is moving in from its maximum open position in (a), is approaching the minimum open position in (b), and is moving outward in (c).

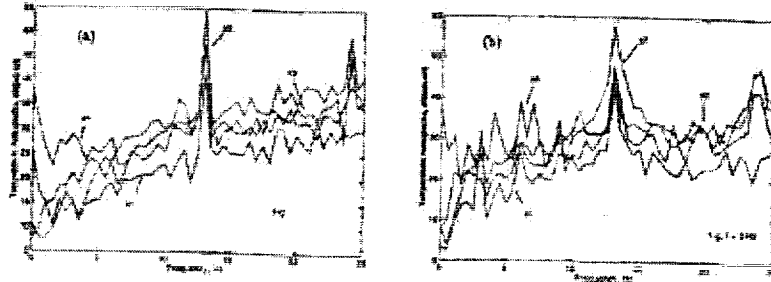


Fig. 8. Temperature autospectra in normal gravity at 1 atm for (a) unpulsed flame, and (b) pulse frequency of 1 Hz. Four thermocouple locations along the flame centerline are shown. Here, x_1 , x_2 , x_3 , and x_4 correspond, respectively, to $x/d = 9, 30, 55$, and 91 ; x is the downstream distance and d is the nozzle diameter.

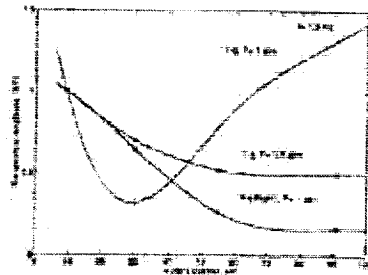


Fig. 9. Variation of temperature amplitude (pulse frequency of 1.5 Hz) for the flames in microgravity ($P = 1.0$ atm) and normal gravity ($P = 0.5$ atm and 1.0 atm). The data are shown for the thermocouple at $x/d = 9$, where x is the downstream distance along the flame centerline and d is the nozzle diameter.